LETTER

doi:10.1038/nature11936

Mesoporous TiO_2 single crystals delivering enhanced mobility and optoelectronic device performance

Edward J. W. Crossland[1], Nakita Noel[1], Varun Sivaram[1], Tomas Leijtens[1], Jack A. Alexander-Webber[1] & Henry J. Snaith[1]

Mesoporous ceramics and semiconductors enable low-cost solar power, solar fuel, (photo)catalyst and electrical energy storage technologies[1]. State-of-the-art, printable high-surface-area electrodes are fabricated from thermally sintered pre-formed nanocrystals[2–5]. Mesoporosity provides the desired highly accessible surfaces but many applications also demand long-range electronic connectivity and structural coherence[6]. A mesoporous single-crystal (MSC) semiconductor can meet both criteria. Here we demonstrate a general synthetic method of growing semiconductor MSCs of anatase TiO_2 based on seeded nucleation and growth inside a mesoporous template immersed in a dilute reaction solution. We show that both isolated MSCs and ensembles incorporated into films have substantially higher conductivities and electron mobilities than does nanocrystalline TiO_2. Conventional nanocrystals, unlike MSCs, require in-film thermal sintering to reinforce electronic contact between particles, thus increasing fabrication cost, limiting the use of flexible substrates and precluding, for instance, multijunction solar cell processing. Using MSC films processed entirely below 150 °C, we have fabricated all-solid-state, low-temperature sensitized solar cells that have 7.3 per cent efficiency, the highest efficiency yet reported. These high-surface-area anatase single crystals will find application in many different technologies, and this generic synthetic strategy extends the possibility of mesoporous single-crystal growth to a range of functional ceramics and semiconductors.

Previous approaches to growing MSC semiconductors aimed at crystallizing the target material from thermal decomposition of precursor species infiltrated into the pores of a sacrificial template[7–17]. However, with the exception of surface-masked epitaxial growth from pre-grown crystal wafers[18], these approaches have achieved ambiguous success in realizing extended MSC semiconductors. Very often the resulting material is best described as a 'mesocrystal'—a porous assembly of nanoscale crystallites with common orientation but no single coherent atomic domain (the classical basis for a single crystal)[19,20]. The external shapes of such templated mesocrystals are spherical or otherwise irregular and do not express the underlying symmetry and facets of the crystal lattice, as is the case for non-porous single crystals. A classical route to large single crystals is growth in a dilute solution[21] and/or at reduced temperatures that lower the rate of nucleation and growth. At first this approach seems incompatible with a templating strategy because without a template volume that encompasses the entire reaction volume, only a vanishingly small number of crystals nucleate inside the template rather than in the bulk solution.

Here we demonstrate that the critical issue of confining growth to the guiding template in the dilute regime is solved by 'seeding' the template with microscopic nucleation sites for crystal growth, which then overwhelms homogeneous nucleation. The specific semiconductor crystals we report are structural inverses of a quasi-close-packed array of silica beads, with pore size tunable from 20 nm to 250 nm. By seeding this template, we achieve a near-unity yield of clearly faceted, high-surface-area single crystals of anatase TiO_2, whose external dimensions grow to orders of magnitude larger than their internal mesopores. There is no longer any need to overcome an energetic barrier to homogeneous nucleation, so the reaction temperature can be lowered significantly such that 'soft' materials like mesoporous block copolymers[22] become suitable host templates for fully crystalline functional ceramics. We propose that this general strategy is applicable to an enormous range of template morphologies and functional materials, from both solution and vapour-phase reactions, and has broad scope in functional ceramics and materials for energy generation and storage.

The anatase TiO_2 MSC growth is based on the synthesis of Yang *et al.*[23] via hydrothermal treatment of TiF_4 in the presence of hydrofluoric acid, which stabilizes the precursor and significantly reduces the nucleation rate[24,25]. A silica template with an external volume that is approximately 1% of the overall reaction volume is first seeded by pre-treatment in a solution of $TiCl_4$ before its immersion in the reaction vessel. The template is finally removed by selective etching in aqueous NaOH to recover the mesoporous TiO_2 crystal product, as illustrated in Fig. 1 (see Methods). Scanning electron microscope (SEM) characterization of the product (Fig. 1d–g) reveals faceted truncated bipyramidal crystals with external symmetry matching that of the homogeneously nucleated bulk crystals (Fig. 1c), whose mesoscale structure is a negative replica of the silica template. The crystal in Fig. 1d is particularly instructive, because it evidently grew from a seed located on or close to an external surface of the mesoporous template. In one direction the crystal growth is directed outwards into the solution and results in a compact, faceted TiO_2 crystal with a symmetry consistent with the anatase TiO_2 Wulff construction. In the opposite direction the growth front enters the templated volume such that the crystal grows around the guiding template (mesoscale detail shown in Fig. 1e). The single set of external crystal facets is strong evidence for the nucleation and growth mechanism of a single-crystal domain from a single nucleation site. Crystals grown entirely within the template pores (Fig. 1f and g) also have external symmetry matching the Wulff construction, now coupled with an internal mesopority whose accessibility is confirmed by dye adsorption–desorption surface area measurements of 150 $\mu m^2\,\mu m^{-3}$ or, equivalently, 70 $m^2\,g^{-1}$ for 20 nm pores in 2 μm^3 crystals. That is, the specific free surface of these MSCs is very similar to equivalent-sized nanoparticles (Dyesol DSL 18NR-T, 20 nm average particle size, 75 $m^2\,g^{-1}$).

Crucially, in the absence of seeding, the overwhelming majority of crystals nucleate and grow outside the template in the solution bulk, producing non-porous crystals of the type shown in Fig. 1c. The relative yield of non-seeded porous crystals is extremely low: only a careful inspection of the etched template product (a transparent solution containing no visible product) by SEM reveals a trace number of porous crystals that nucleate homogeneously inside the silica template. The total number of homogeneously nucleated crystals without seeding (N_0) follows from the average crystal volume and total TiO_2 product mass and is approximately 5×10^8. After seeding the template in 15 μM aqueous $TiCl_4$, however, the number of crystals increases to about 9×10^{10}—a nucleation rate roughly two orders of magnitude greater than the homogeneous rate. Seeded growth dominates homogeneous

[1]Clarendon Laboratory, University of Oxford Parks Road, Oxford, OX1 3PU, UK.

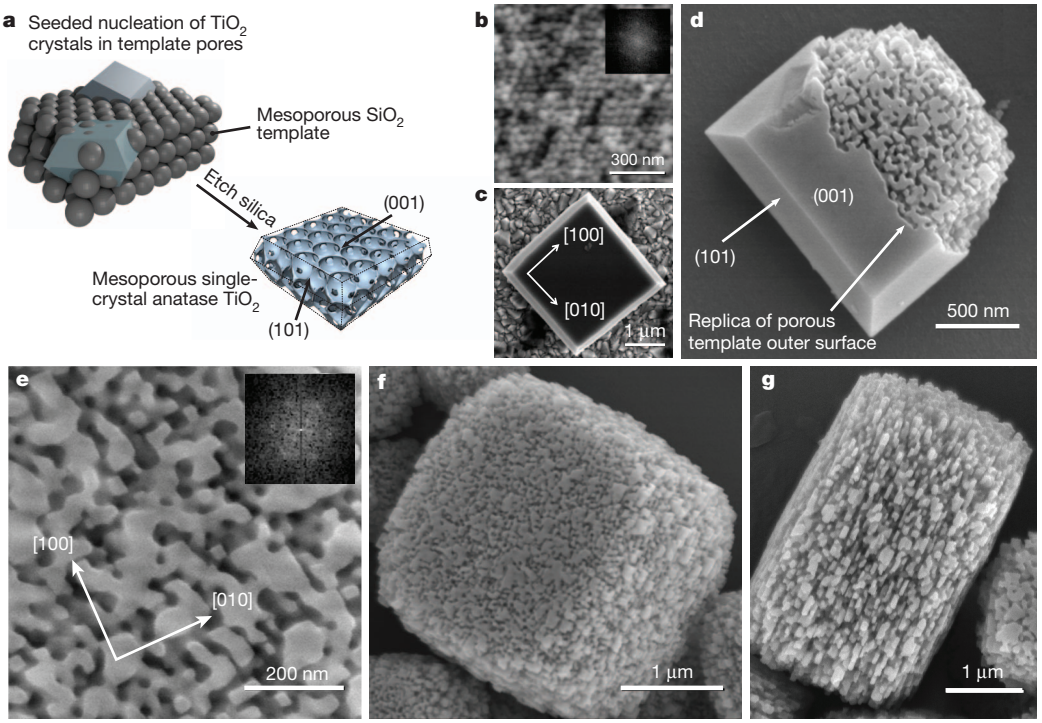

Figure 1 | MSC synthesis of TiO_2. **a**, Schematic of MSC nucleation and growth within a mesoporous template. **b**, Pristine silica template made up of quasi-close-packed silica beads (fast Fourier transform (FFT) inset showing sixfold symmetry with 49 ± 3 nm spacing). **c**, Non-porous truncated bipyramidal TiO_2 crystal homogeneously nucleated in a 20-mM TiF_4 solution at 210 °C. **d**, Template-nucleated variant of the crystal type shown in **c**, grown from a seed at or near the external template surface such that a non-porous volume coexists with a mesoporous region within a single faceted microcrystal. **e**, Replication of the mesoscale pore structure within the templated region (FFT inset, 47 ± 3 nm sixfold symmetry) with crystal lattice vectors implied from the particle symmetry overlaid (reaction conditions 170 °C, 40 mM TiF_4). **f** and **g**, Fully mesoporous TiO_2 crystals grown by seeded nucleation in the bulk of the silica template.

nucleation and the vast majority of TiO_2 crystals grow inside the template rather than in the bulk solution, giving a near-unity yield of mesoporous crystals.

We further probed the nature of the templated crystals at the atomic scale by X-ray diffraction (XRD) and electron diffraction, shown in Fig. 2. The X-ray diffraction pattern of an ensemble of the mesoporous product is compared in Fig. 2a to both a standard mesoporous anatase TiO_2 nanoparticle film (Dyesol DSL 18NR-T, 20 nm average particle size) and to non-templated (solid) anatase microcrystals. All patterns index to the anatase phase of titania. The apparent average domain size of the conventional nanoparticle film calculated from Scherrer broadening of the primary (101) peak is 20 nm. The peak width of the TiO_2 crystals synthesized from the TiF_4 precursor is very much narrower, and is now limited by the machine broadening of 0.08° full width at half maximum. Importantly, the peak width of the mesoporous crystals, with 20 nm porosity, matches that of the non-templated anatase microcrystals, consistent with the porous particles being single-crystal domains; this correspondence is independent of pore size, consistent with a decoupling of crystallinity and surface area (Supplementary Information).

Electron diffraction taken from complete mesoporous particles produces the Laue diffraction patterns shown in Fig. 2c and e that are indexed to anatase TiO_2 with beam orientation consistent with the crystal symmetry of the Wulff construction. The distinct crystal shapes in Fig. 2b and d result from different reaction temperatures (described in detail in the Supplementary Information). Taken together with SEM characterization of particle size and symmetry, these results are entirely consistent with the mesoporous particles comprising a single underlying anatase crystal domain, with missing internal volume defined by the mesoporous template—we therefore refer to this material as a mesoporous single crystal (MSC), and it is, to the best of our knowledge, the first such example for anatase TiO_2.

We now return to the question of seeding density, which can be used not only to increase the relative number of crystals that grow in the template, but also to control their size, given that the seeded crystals grow in parallel, consuming all the available Ti precursor if the reaction is run to completion. In Fig. 3 we show how the number of TiO_2 seeds (N) and hence the average crystal volume (inversely proportional to N) can be varied over four orders of magnitude by varying the $TiCl_4$ seeding solution concentration from 15 μM to 15 mM. The Ti content in the seeded template, determined by inductively coupled plasma atomic emission spectroscopy (ICPOES), increases approximately linearly with $[TiCl_4]$ in this range (see ICPOES results and corresponding SEM images in the Supplementary Information). This result demonstrates explicitly how the MSC domain size is decoupled from the internal pore dimension imposed by the template morphology.

As an alternative to varying seed density, we can control both MSC size and shape via the TiF_4 hydrothermal reaction conditions. Reaction temperature, for example, influences both the aspect ratio and lateral size of the MSCs for a fixed template morphology, seed density and reaction time. We can adjust the internal mesopore size by replicating silica bead templates of different diameter d, such that the surface area (in square metres per gram) of the quasi-close-packed templates is inversely proportional to d. We show MSC pore morphologies replicating bead diameters between 20 nm and 250 nm in the Supplementary Information. Control over the mesopore dimension is important not only for increasing specific surface area, but also for optimizing diffusion of species through the pore structure in, for example, high-efficiency dye-sensitized solar cells (SSCs) containing viscous liquid electrolytes or solid-state hole-conductors and for long-range ion diffusion in batteries[2].

We have demonstrated a synthesis protocol for anatase TiO_2 MSCs with independently tunable crystal and pore size. We now investigate whether they genuinely exhibit superior electronic properties in

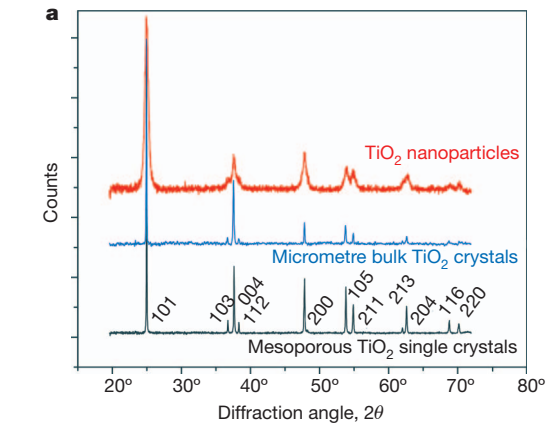

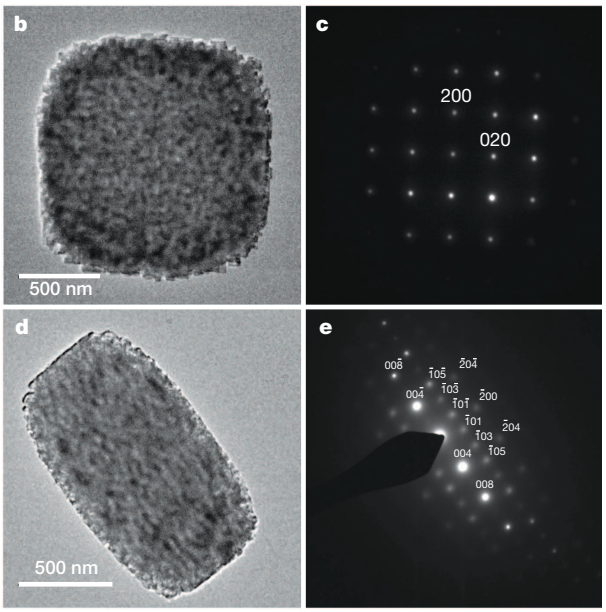

Figure 2 | X-ray and electron diffraction of mesoporous TiO_2 crystals. **a**, X-ray diffraction patterns of an ensemble of mesoporous TiO_2 crystals with 20-nm pore size and the equivalent non-templated microcrystals, compared to an ensemble of anatase nanoparticles (Dyesol DSL 18NR-T, 20-nm average particle size). **b** and **c**, Transmission electron micrograph (**b**) and electron diffraction Laue pattern (**c**) collected from a complete mesoporous crystal (synthesized at 190 °C, 40 mM TiF_4) assigned to anatase TiO_2 with [001] beam incidence. **d** and **e**, Equivalent image and Laue pattern for crystals synthesized at 130 °C, 120 mM TiF_4, indexed with [010] or [100] incidence.

comparison to mesoporous films constructed from dried or sintered nanoparticles. We first measure the electronic conductivity through an isolated MSC and compare it to that of TiO_2 nanoparticle films, summarizing the results in Fig. 4a. Before and after annealing at 500 °C, the MSC exhibits conductivity just under three and two orders of magnitude higher, respectively, across an approximately 500-nm electrode gap. The nanoparticle film conductivity increases far more upon sintering than does that of the MSC, rationalized by enhanced electronic contact through neck growth between the nanoparticles—a process now less relevant to MSCs because of pre-existing long-range crystal order[3,26]. Notably, the as-cast MSC is more conductive than the sintered nanoparticle film.

We also estimate the electronic mobility in MSC films, for which we have recently developed the requisite technique, which we call 'transient mobility spectroscopy'. Briefly, we measure the time-resolved conductivity and photoinduced charge absorption simultaneously to extract the charge density and hence mobility. In this configuration, the electrode gap is approximately 300 μm, so the measured MSC mobility is an effective mobility including the influence of interparticle boundaries.

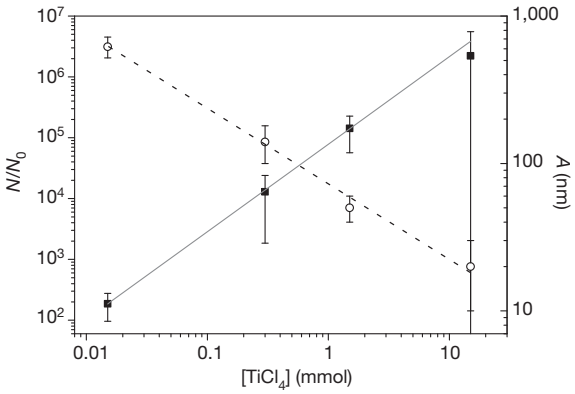

Figure 3 | MSC size control via nucleation seed density. MSC dimension A (circles) and inferred ratio of seed nuclei N to homogeneous nucleation N_0 as a function of $TiCl_4$ pre-treatment concentration (squares). Lines are drawn to guide the eye. Error bars for A represent one standard deviation of the measured sample distribution (minimum 100 samples). Primary hydrothermal reaction conditions were: 210 °C, 12 h, 20 mM TiF_4, in all cases.

Despite this, the MSC films exhibit mobility values over an order of magnitude higher than those of the nanoparticle films over a broad range of charge densities (Fig. 4b).

We have clearly demonstrated the advantageous electronic properties of the MSCs versus nanoparticle films, along with the unique property that MSC electron transport is highly effective even without any on-film heat treatment or sintering process. To capitalize on this commercially attractive property, we have used films of MSCs (300 nm crystal size to facilitate smooth film deposition) in low-temperature solid-state SSCs. All-solid-state SSCs, as opposed to those containing liquid electrolytes, suffer from fast electron–hole recombination, and the highest full sun power conversion efficiency reported for a solid-state SSC where all components are processed under 150 °C is a little over 1% (ref. 27). In Fig. 4c, we present current–voltage curves measured under simulated AM1.5 100 mW cm^{-2} sunlight for sub-150 °C processed SSCs using the organic dye sensitizer D102 or a mixed-halide organometallic perovskite sensitizer, $CH_3NH_3PbI_2Cl$ (refs 5, 28). The dye-sensitized cell achieves a 3% power conversion efficiency, comparable to the highest reported value of 4.1% for high-temperature-processed D102-sensitized anatase nanoparticles and vastly greater than the previous best low-temperature all-solid-state SSC[27]. MSCs coupled with the more effective perovskite light harvester deliver double the current and a power conversion efficiency of over 7%, higher than any reported low-temperature SSC architecture and competitive with high-temperature devices[5].

We have thus demonstrated a novel, highly effective, and versatile method for synthesizing micrometre-size mesoporous single-domain semiconductor particles based on crystal seeding in a sacrificial guiding template. Here we prove that this technique works very well for anatase TiO_2 in silica pores, but this method should be quite generally applicable to other functional ceramics and semiconductors. The complete decoupling of crystal size (atomic-scale order) from mesoscale porosity also provides an ideal system for fundamental investigation into the electronic processes in porous semiconductors. In addition, the accessibility of the exposed surface area opens up new possibilities for controlled surface treatments and solution-based core–shell synthesis, potentially decoupling long-range electronic and surface properties.

We have also demonstrated the promise held by MSCs for a specific application—SSCs. MSCs display higher conductivity and electron mobility than conventionally used nanocrystalline TiO_2, and the elimination of thermal sintering treatment enabled us to fabricate a solid-state SSC that attained a record 7.2% efficiency for sub-150 °C processing. This instantly opens up possibilities for multi-junction device fabrication, broadens substrate choice, and reduces manufacturing steps and costs for SSCs. More generally, incorporation of a

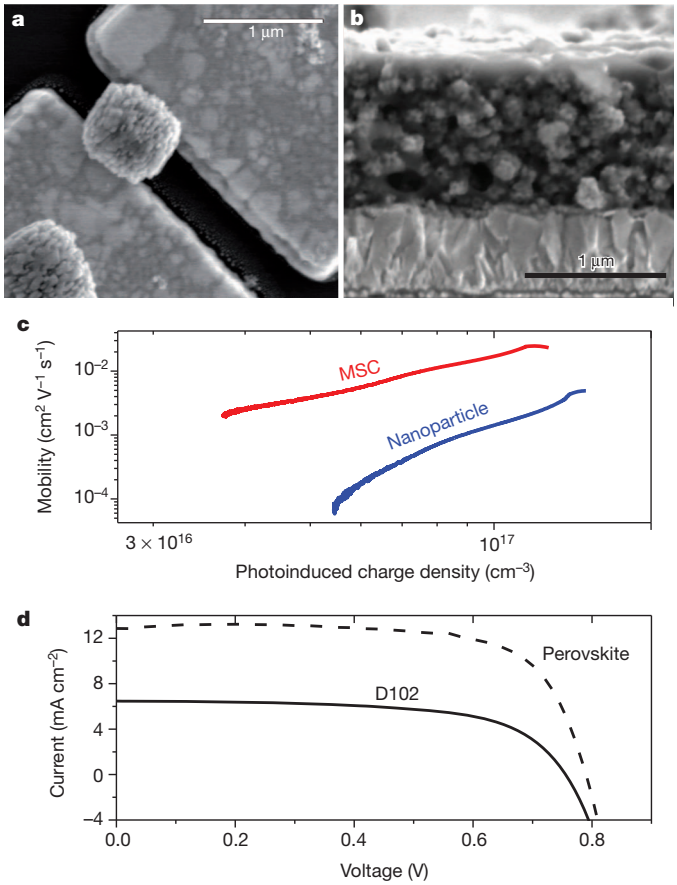

Figure 4 | Electronic properties and device performance of MSCs. a, SEM image of an MSC spanning a gold electrode gap. The conductivity of an isolated MSC is 4.9×10^{-6} S cm^{-1} before sintering at 500 °C and 1.5×10^{-5} S cm^{-1} afterwards. The conductivity of TiO_2 nanoparticle films before sintering at 500 °C is 8.4×10^{-9} S cm^{-1}and 2.2×10^{-7} S cm^{-1}afterwards. **b**, SEM cross-section of a solid-state dye-sensitized solar cell comprised of MSCs. **c**, Mobility dependence on photoinduced charge density for MSC and nanoparticle films measured via transient mobility spectroscopy. **d**, Current–voltage curves of all-low-temperature solid-state SSCs using MSC photoanodes with either the D102 dye or the perovskite sensitizer. The D102 device shows an efficiency of 3.11%, a short-circuit current of 6.47 mA cm^{-2}, an open-circuit voltage of 0.76 V and a fill factor of 0.63. The perovskite device shows an efficiency of 7.29%, a short-circuit current of 12.86 mA cm^{-2}, an open-circuit voltage of 0.79 V and a fill factor of 0.70.

variety of MSCs into active device layers should lead to great advances in operational efficiency of mesostructured solar cells, arising from rapid charge extraction in the inorganic phase, and improved battery operation due to enhanced charging and discharging rates.

METHODS SUMMARY

Mesoporous silica templates. Silica spheres were synthesized according to ref. 29 and collected by centrifugation. The template was seeded by immersion in aqueous $TiCl_4$ (15 μM to 15 mM) at 70 °C for 60 min followed by thorough rinsing with 1 litre H_2O.

TiO_2 MSC synthesis. Titanium tetrafluoride was dissolved (20 mM to 400 mM) in water (pH 2.1) to which was added the ionic liquid 1-methylimidazolium tetrafluoroborate (180 mM), and 650 mg of the pre-treated silica template for 50 ml of TiF_4 solution in a 125-ml-volume autoclave lined with Teflon (PTFE, poly(tetrafluroethane); Parr Instruments). The silica template was selectively etched in 2 M aqueous NaOH at 80 °C for 60 min in a polypropylene beaker and the TiO_2 product collected by centrifugation (3,000 r.p.m. for 60 min) and washed several times in water and ethanol.

Low-temperature solar cell assembly. Solid-state dye-sensitized solar cells were fabricated following the general process described in detail elsewhere[30]. A TiO_2 compact layer was first deposited by spin-coating a titanium isopropoxide solution in ethanol and dried at 150 °C. TiO_2 MSCs were deposited from suspension in ethanol containing 15 mol.% titanium diisopropoxide bis(acetylacetonate) relative to TiO_2, before sensitization with the D102 organic dye or coating with the perovskite precursor solution[5]. A Spiro-OMeTAD (2,2′7,7′-tetrakis-(N,N-dipmethoxyphenylamine)9,9′-spirobifluorene) hole transporter layer was deposited by spin-coating from cholorobenzene solutions containing tert-butylpyridine and lithium-bis(trifluoromethanesulphonyl)imide (TFSI) additives. 200-nm-thick silver counter electrodes were thermally evaporated over the hole transporter.

Characterization methods. Template and crystal-replica morphologies were investigated by SEM (Hitachi S-4300) at an accelerating voltage of 5 kV after platinum coating samples prepared by drop casting on glass substrates. Transmission electron microscope measurements were made with a Jeol2010 microscope operating at 200 kV. Dye desorption–adsorption measurements were conducted by sensitizing a thin layer of TiO_2 in the ruthenium dye N719 for 12 h. The dye was desorbed and its concentration evaluated from the peak optical absorption at 500 nm. Current–voltage characteristics of solar cells were measured under AM1.5 light at 100 mW cm^{-2} generated using an ABET Technologies solar simulator calibrated using a National Renewable Energy Laboratories (NREL) calibrated silicon reference cell with a KG5 filter to minimize spectral mismatch. Current–voltage curves were measured with a Keithley 2400 unit. All devices were masked with a metal aperture to define the active area and to eliminate edge effects. MSC conductivity measurements were taken using two-probe contact to gold electrodes with a single MSC crystal bridging the gap between them.

Full Methods and any associated references are available in the online version of the paper.

Received 11 December 2012; accepted 23 January 2013.
Published online 6 March 2013.

1. Weickert, J., Dunbar, R. B., Hesse, H. C., Wiedemann, W. & Schmidt-Mende, L. Nanostructured organic and hybrid solar cells. *Adv. Mater.* **23,** 1810–1828 (2011).
2. Yella, A. *et al.* Porphyrin-sensitized solar cells with cobalt (II/III) based redox electrolyte exceed 12 percent efficiency. *Science* **334,** 629–634 (2011).
3. O'Regan, B. & Grätzel, M. A low-cost, high-efficiency solar cell based on dye-sensitized colloidal TiO_2. *Nature* **353,** 737–740 (1991).
4. Grätzel, M. Photoelectrochemical cells. *Nature* **414,** 338–344 (2001).
5. Lee, M. M., Teuscher, J., Miyasaka, T., Murakami, T. N. & Snaith, H. J. Efficient hybrid solar cells based on meso-superstructured organometal halide perovskites. *Science* **338,** 643–647 (2012).
6. Docampo, P., Guldin, S., Steiner, U. & Snaith, H. J. Charge transport limitations in self-assembled TiO_2 photoanodes for solid-state dye-sensitized solar cells. *J. Phys. Chem. Lett.* http://dx.doi.org/10.1021/jz400084n (in the press).
7. Schüth, F. Endo- and exotemplating to create high-surface-area inorganic materials. *Angew. Chem. Int. Edn* **42,** 3604–3622 (2003).
8. Lu, A.-H. & Schüth, F. Nanocasting: a versatile strategy for creating nanostructured porous materials. *Adv. Mater.* **18,** 1793–1805 (2006).
9. Dickinson, C. *et al.* Formation mechanism of porous single-crystal Cr_2O_3 and Co_3O_4 templated by mesoporous silica. *Chem. Mater.* **18,** 3088–3095 (2006).
10. Tian, B. *et al.* General synthesis of ordered crystallized metal oxide nanoarrays replicated by microwave-digested mesoporous silica. *Adv. Mater.* **15,** 1370–1374 (2003).
11. Yue, W. & Zhou, W. Synthesis of porous single crystals of metal oxides via a solid–liquid route. *Chem. Mater.* **19,** 2359–2363 (2007).
12. Yang, P., Zhao, D., Margolese, D. I., Chmelka, B. F. & Stucky, G. D. Generalised synthesis of large-pore mesoporous metal oxides with semicrystalline frameworks. *Nature* **396,** 152–155 (1998).
13. Li, D., Zhou, H. & Honma, I. Design and synthesis of self-ordered mesoporous nanocomposite through controlled in-situ crystallization. *Nature Mater.* **3,** 65–72 (2004).
14. Yu, J. C., Wang, X. & Fu, X. Pore-wall chemistry and photocatalytic activity of mesoporous titania molecular sieve films. *Chem. Mater.* **16,** 1523–1530 (2004).
15. Kondo, J. N. & Domen, K. Crystallization of mesoporous metal oxides. *Chem. Mater.* **20,** 835–847 (2008).
16. Yue, W. & Zhou, W. Crystalline mesoporous metal oxide. *Prog. Nat. Sci.* **18,** 1329–1338 (2008).
17. Jiao, K. *et al.* Growth of porous single-crystal Cr_2O_3 in a 3D mesopore system. *Chem. Commun.* 5618–5620 (2005).
18. Arora, H. *et al.* Block copolymer self-assembly-directed single-crystal homo- and heteroepitaxial nanostructures. *Science* **330,** 214–219 (2010).
19. Yue, W. *et al.* Mesoporous monocrystalline TiO_2 and its solid-state electrochemical properties. *Chem. Mater.* **21,** 2540–2546 (2009).
20. Bian, Z. *et al.* Single-crystal-like titania mesocages. *Angew. Chem. Int. Edn* **50,** 1105–1108 (2011).
21. Finnemore, A. S. *et al.* Nanostructured calcite single crystals with gyroid morphologies. *Adv. Mater.* **21,** 3928–3932 (2009).
22. Crossland, E. J. W. *et al.* A bicontinuous double gyroid dye-sensitized solar cell. *Nano Lett.* **9,** 2807–2812 (2009).

23. Yang, H. G. *et al.* Anatase TiO_2 single crystals with a large percentage of reactive facets. *Nature* **453,** 638–641 (2008).
24. Zhang, D., Li, G., Yang, X. & Yu, J. C. A micrometer-size TiO_2 single-crystal photocatalyst with remarkable 80% level of reactive facets. *Chem. Commun.* 4381–4383 (2009).
25. Liu, G., Yu, J. C., Lu, G. Q. M. & Cheng, H.-M. Crystal facet engineering of semiconductor photocatalysts: motivations, advances and unique properties. *Chem. Commun.* **47,** 6763–6783 (2011).
26. Nakade, S. *et al.* Dependence of TiO_2 nanoparticle preparation methods and annealing temperature on the efficiency of dye-sensitized solar cells. *J. Phys. Chem. B* **106,** 10004–10010 (2002).
27. Jiang, C. Y. *et al.* Low temperature processing solid-state dye sensitized solar cells. *Appl. Phys. Lett.* **100,** 113901 (2012).
28. Schmidt-Mende, L. *et al.* Organic dye for highly efficient solid-state dye-sensitized solar cells. *Adv. Mater.* **17,** 813–815 (2005).
29. Bogush, G. H., Tracy, M. A. & Zukoski, C. Z. IV Preparation of monodisperse silica particles: control of size and mass fraction. *J. Non-Cryst. Solids* **104,** 95–106 (1988).
30. Docampo, P. *et al.* Control of solid-state dye-sensitized solar cell performance by block-copolymer-directed TiO_2 synthesis. *Adv. Funct. Mater.* **20,** 1787–1796 (2010).

Supplementary Information is available in the online version of the paper.

Acknowledgements This work was funded by the European Community's Seventh Framework Programme (FP7/2007-2013) under grant agreement number 246124 of the SANS project, the European Research Council (HYPER project number 279881), the Rhodes Trust, the Engineering and Physical Sciences Research Council, and the Government of the Republic of Trinidad and Tobago. We thank C. Ducati for help with indexing of electron diffraction patterns.

Author Contributions E.J.W.C. and H.J.S. conceived the idea of the project. E.J.W.C. devised and performed materials synthesis and characterization. N.N. and V.S. fabricated and characterized solar cells and optoelectronic devices. T.L. and J.A.A.-W. contributed to electronic mobility measurements. E.J.W.C., H.J.S. and V.S. wrote the manuscript. All authors commented on the manuscript. H.J.S. supervised the project.

Author Information Reprints and permissions information is available at www.nature.com/reprints. The authors declare no competing financial interests. Readers are welcome to comment on the online version of the paper. Correspondence and requests for materials should be addressed to H.J.S. (h.snaith1@physics.ox.ac.uk).

METHODS

Preparation of mesoporous silica templates. Silica spheres were synthesized according to ref. 29. For example, 50-nm spheres were synthesized by adding 32 ml H_2O (Millipore 18M Omega), 18 ml ammonium hydroxide (30%, Sigma Aldrich) and 99 ml tetraethyl orthosilicate (TEOS, Sigma Aldrich) to 750 ml ethanol and stirred at 700 r.p.m. for 24 h. A quasi-close-packed bead template was prepared by centrifugation of the reaction solution (7,000 r.p.m., 5 h) leaving a translucent solid. The (unwashed) solid was sintered at 500 °C for 30 min (ramping time 150 min).

Pre-seeding of silica templates. An aqueous $TiCl_4$ solution (15 μM to 15 mM) was prepared by aqueous dilution of an aqueous 2 M $TiCl_4$ stock solution (stock preparation: 100 ml of $TiCl_4$ (Sigma Aldrich) was added to 350 ml H_2O containing 1 ml of 35% HCl in an ice bath). 5 g of the sintered template was immersed in 33 ml of aqueous $TiCl_4$ and held at 70 °C for 60 min followed by thorough rinsing with 1 litre of H_2O. The dried template was resintered at 500 °C for 30 min (ramping time 150 min). The ratio of titanium to silicon (weight/weight) present in the treated template was determined by inductively coupled plasma optical emission spectrometry after microwave digestion in hydrofluoric acid (ICPOES, Exeter Analytical).

TiO_2 MSC synthesis. Mesoporous TiO_2 crystals were synthesized hydrothermally using a modified version of the procedure reported in ref. 24. Titanium tetrafluoride (TiF_4, Alfa Aesar) was dissolved in 18 MΩ H_2O (at concentrations from 20 mM to 400 mM) after first adjusting the pH to 2.1 by addition of 37% HCl (200 μl in 250 ml). 1.67 ml of the ionic liquid 1-methylimidazolium tetrafluoroborate, and 650 mg of the pre-treated silica template were added to 50 ml of TiF_4 solution in a 125-ml-volume Teflon-lined autoclave (Parr Instruments). The sealed vessel was brought to the target reaction temperature (100–210 °C) in a fan-assisted oven for the period of the reaction before cooling in air over approximately 1 h. The template product was collected as a solid white powder settled at the base of the vessel and rinsed with H_2O by vacuum filtration on 1.2-μm paper (Whatman). The silica template was selectively etched in aqueous 2 M NaOH at 80 °C for 60 min in a polypropylene beaker. The remaining TiO_2 was collected by centrifugation (3,000 r.p.m. for 60 min) and washed twice with 50 ml H_2O, and twice with 50 ml ethanol.

Low-temperature solar cell assembly. Solid-state dye-sensitized solar cells were fabricated following the general process described in detail elsewhere[30], and we describe only deviations from that process here. A TiO_2 compact layer was first deposited by spin-coating on a clean glass substrate coated with fluorine-doped tin oxide. The compact layer spin-coating solution was prepared by adding 0.71 g titanium isopropoxide and 0.07 g HCl to 8 ml of ethanol. After drying the compact layer at 150 °C for thirty minutes, the TiO_2 MSC mesostructure was deposited by spin-coating a solution of MSCs (300 nm crystal size, 50 nm pore size) dispersed in ethanol at 10% concentration by weight with the addition of 15 mol.% titanium diisopropoxide bis(acetylacetonate) relative to TiO_2. The substrates were again dried at 150 °C and subsequently immersed in the sensitizing solution containing D102 organic dye for one hour, or coated with the perovskite precursor solution described elsewhere[5]. After sensitization the Spiro-OMeTAD hole transporter layer was deposited by spin-coating from chlorobenzene at a concentration of 180 mg ml^{-1}, along with tert-butylpyridine and lithium-TFSI additives. 200-nm-thick silver counter electrodes were thermally evaporated over the hole transporter.

Characterization methods. Template and crystal-replica morphologies were investigated by SEM (Hitachi S-4300) at an accelerating voltage of 5 kV after platinum coating (3 nm) samples prepared by drop casting on glass substrates. Transmission electron microscope measurements were made with a Jeol2010 microscope operating at 200 kV. Dye desorption–adsorption measurements were conducted by sensitizing a thin layer of TiO_2 by immersion in a 10 mM solution (1:1 by volume of acetonitrile and tert-butanol) of the ruthenium dye N719 for 12 h. The dye was desorbed after thorough rinsing of the film in acetonitrile using a known volume of 200 mM aqueous KOH and the concentration evaluated from the peak absorption at 500 nm assuming a molar absorptivity coefficient of 14,000 M^{-1} cm^{-1} and effective area per molecule[31] of 1.8 nm^2. To obtain the current–voltage characteristics of low-temperature MSC-based solar cells, AM1.5 light at 100 mW cm^{-2} was generated using an ABET Sun 2000 class AAB solar simulator calibrated using an NREL calibrated silicon reference cell with a KG5 filter to minimize spectral mismatch. Current–voltage curves were measured with a Keithley 2400 unit. The solar cells were masked with a metal aperture to define the active area and to eliminate any edge effects. MSC conductivity measurements were taken using two-probe contact to gold electrodes with a single MSC bridging the gap between. To accomplish this, several pairs of gold electrodes were fabricated on silicon dioxide/silicon substrates using electron beam lithography, such that the electrodes could be contacted macroscopically, but narrowed to a width of 2.5 μm with a separating gap of 500 nm (see Fig. 4a). Subsequently, MSCs dissolved in ethanol were dropcast on the silicon substrate, dried and examined under an SEM to confirm the precise geometric parameters of any gap-bridging crystals present. Transient mobility spectroscopy will be described in detail elsewhere. Briefly, pump–probe spectroscopy is used to monitor the absorption signature of the photo-injected charge in the device. Conductivity devices are fabricated as described above with C106 sensitizing dye and no hole transporter. The pump wavelength is 550 nm to excite the dye molecules and induce photo-injection of electrons, whereas the probe wavelength of 900 nm measures the population of dye cations; simultaneously, the in-plane conductivity is measured. This allows the extraction of conductivity and photoinduced charge density as a function of time, from which the charge mobility can be calculated.

31. Zakeeruddin, S. M. *et al.* Design, synthesis, and application of amphiphilic ruthenium polypyridyl photosensitizers in solar cells based on nanocrystalline TiO_2 films. *Langmuir* **18,** 952–954 (2002).